ACS Macro Letters

Letter

pubs.acs.org/macroletters

Chain-Folding Structure of a Semicrystalline Polymer in Bulk Crystals Determined by $^{13}C-^{13}C$ Double Quantum NMR

You-lee Hong and Toshikazu Miyoshi*

Department of Polymer Science, The University of Akron, Akron, Ohio 44325, United States

Supporting Information

ABSTRACT: A unique approach using $^{13}C-^{13}C$ double quantum (DQ) NMR combined with selective ^{13}C isotope labeling is proposed to investigate the chain trajectory of the synthetic polymer in bulk crystals. Since the DQ buildup curve highly depends upon coupled spin number, topology, and internuclear distance, which originated from the chain trajectory of selectively ^{13}C-labeled polymers, the adjacent re-entry site and fraction under finite chain-folding number can be determined.

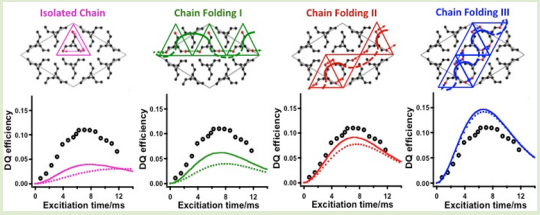

Since the discovery of single crystals of polyethylene (PE) by Keller using transmission electron microscopy (TEM),[1] various methods including neutron scattering (NS)[2,3] and IR[4] combined with ^{2}H polymers and monodisperse oligomers,[5] surface decoration,[6] and direct observation[7] and force detection[8] of single chains using atomic force microscopy (AFM) have been developed to unravel detailed chain-level structures (chain trajectory) of semicrystalline polymers in single as well as bulk crystals. It is still challenging, however, to properly reveal (i) the adjacent re-entry fraction, (ii) the re-entrance site of folded chains, and (iii) the number of chain-folding in real polymer crystals. Recent computer simulations have successfully investigated molecular level structures of individual chains during crystallization.[9,10] Monte Carlo Dynamic (MD) simulation by Hu et al.[9] showed that the bead model of polyethylene includes a large amount of adjacent re-entry structures even in the bulk state. Further MD simulations by Sommer et al.[10] indicated that polyvinyl alcohol (CG-PVA) random chains in molten states of the coarse-grained model are folded for a very short time (ca. a few picoseconds) in the pre-stage of crystallization. Both results suggest that intrachain interactions via adjacent re-entry structure play dominant roles for the nucleation of polymer crystals. To accurately determine how intrachain interactions influence the nucleation of polymer crystals, however, experimental techniques must be developed to elucidate chain structure and validate results of simulations.

Solid-state NMR (SS-NMR) is one of the most powerful tools to characterize molecular structures and dynamics of organic as well as inorganic systems.[11,12] Among various magnetic interactions, the dipolar interaction, which is inversely proportional to the third power of internuclear distance, $1/\langle r\rangle^3$, has been successfully applied to investigate local structures such as chain conformation,[13] packing,[14] and intra- and intermolecular interactions.[15−17] Multiple distance measurements combined with spin dilution have been used to determine three-dimensional structures of protein fragments in solid states.[18] In this communication, chain-folding structures such as (i) re-entrance sites, (ii) adjacent re-entry fraction (F), and (iii) chain-folding number (n) of a polymer in bulk crystals are investigated for the first time by $^{13}C-^{13}C$ double quantum (DQ) NMR combined with selective ^{13}C isotope labeling. In this work, the adjacent re-entry fraction is defined as a fraction of the number of ^{13}C-labeled stems within adjacent re-entry structures relative to the number of all ^{13}C-labeled stems in a sample.

^{13}C 30% CH_3-labeled *isotactic* poly(1-butene) (iPB1) (M_w = 26 215 g/mol and isotacticity [*mmmm*] = 96.6%) was synthesized. The sample, crystallized in the bulk state at T_c = 95 °C, gives a high crystallinity of 88% (see Figure S1, Supporting Information), lamellae thickness of $\langle l\rangle$ = 20 nm,[19] and a melting temperature of 126 °C. The chains in form I of iPB1 adopt 3_1 helical conformations in a trigonal lattice ($a = b$ = 17.7 ± 0.1 Å and c = 6.5 ± 0.1 Å) (Figure 1(a)).[20] On the basis of M_w and $\langle l\rangle$, the maximum folding number (n_{max}) is calculated to be 4. The closest CH_3-CH_3 carbon distance between the neighboring stems is much shorter (4.2 Å) than that within the same stem (6.3 Å) (Figures 1(a) and (b)). Selectively $^{13}CH_3$-labeled iPB1, therefore, is a good candidate to extract chain-folding structures of synthetic polymers. Our experimental approach is schematically illustrated in Figures 1(c) and (d). ^{13}C-labeled chains colored by blue are diluted with nonlabeled chains, and $^{13}C-^{13}C$ DQ NMR experiments are performed, where the acquired DQ buildup curve traces the chain trajectory of isolated ^{13}C-labeled chains as signal intensities. Well-folded chain structures are expected to produce intense DQ signals (Figure 1(c)). In Figure 1(c), the labeled chain adopts adjacent re-entry structures with n = 4 (F = 100%). Random re-entry structures would produce weak DQ signals due to the low probabilities for adjacent re-entry. The model chain colored by blue in Figure 1(d) has F = 0% at n = 2.

Received: December 3, 2012
Accepted: May 22, 2013
Published: May 24, 2013

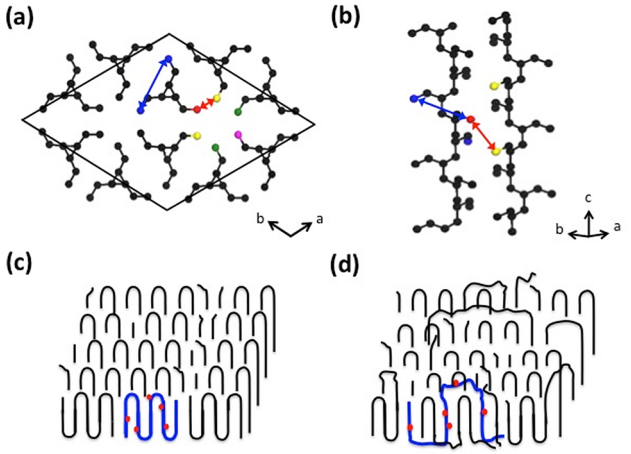

Figure 1. (a) Crystal structure of form I iPB1 on the (011) plane and (b) two chains on side view. The $^{13}C-^{13}C$ shortest internuclear distances between neighboring stems (4.2 Å) and within an intrastem (6.3 Å) determined by XRD[20] are shown as red and blue arrowed lines, respectively. Schematic drawing of (c) adjacent re-entry and (d) random re-entry models. The blue lines and red dots are ^{13}C-labeled chains and atoms, respectively.

NMR experiments were carried out on BRUKER AVANCE III 300, equipped with a 4 mm double resonance probe. The carrier frequencies of ^{1}H and ^{13}C are 300.1 and 75.5 MHz, respectively. The PostC7 sequence was applied for exciting $^{13}C-^{13}C$ DQ signals at a magic-angle spinning (MAS) frequency of 5102 Hz at ambient temperature.[21] High power TPPM and CW decoupling with a field strength of 100 kHz was used during acquisition and recoupling periods, respectively (see Supporting Information). Figure 2(b) illustrates relaxation ($T_{1\rho H}$) filtered ^{13}C single quantum (SQ) (black) and double quantum DQ (red) NMR spectra of 30% $^{13}CH_3$-labeled iPB1 in the crystalline regions. Figure 2(d) displays a $^{13}C-^{13}C$ DQ buildup curve (open circles) of the $^{13}CH_3$ signal as a

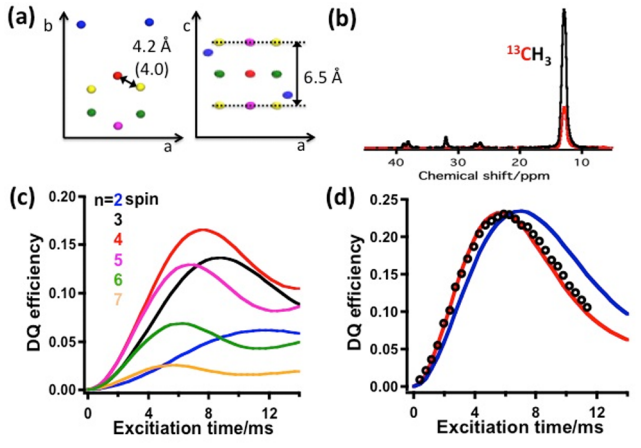

Figure 2. (a) Coordinates of an 11 spin system being used in chain-packing simulation. (b) ^{13}C high-resolution DQ (red) and SQ (black) NMR spectra of 30% $^{13}CH_3$-labeled iPB1 form I at ambient temperature. (c) Calculated DQ efficiency curves for each m spin system with probability (P_m) without a T_2 relaxation effect. (d) Experimental (open circles) and calculated DQ efficiency curves of chain packing based on $\langle r \rangle$ = 4.0 Å and exponential type of T_2 relaxation with 18.5 ms (red line) and $\langle r \rangle$ = 4.2 Å and T_2 = 24 ms (blue line).

function of excitation time (t_{ex}). $^{13}C-^{13}C$ DQ efficiency, ξ, achieves a maximum value (ξ_{max}) of 0.23 at t_{ex} = 5.5 ms. ξ_{max} is governed by $^{13}C-^{13}C$ dipolar interaction, chemical shift anisotropy (CSA), decoupling efficiency, and incoherent T_2 relaxation.[13,17] Strong decoupling can effectively eliminate $^{1}H-^{13}C$ dipolar interaction during $^{13}C-^{13}C$ recoupling. Dipolar interactions and a T_2 relaxation are taken into account in our simulations. The latter, in principle, can contain some contributions from decoupling and CSA.

In our simulation, a reference methyl carbon plus the 10 closest surrounding carbons (8 interstem and 2 intrastem) are considered as a model system for chain-packing analysis (Figures 1(a) and 2(a)). The validity of 11 spin systems will be discussed in the DQ curve of the isolated stem. All the internuclei distances within 8 Å and spin coordinates are depicted in Figure S2 (Supporting Information). The spin colored by red is fixed for detection of DQ signals in numerical simulation by SPINEVOLUTION.[22] The 30% labeling ratio of methyl groups statistically produces different spin systems (number, distance, and topology) among 11 sites. The probability of finding m spins among 11 sites is calculated using a following equation of $P_m = {}_{10}C_{m-1}(x)^{m-1}(1-x)^{10-(m-1)}$, where ${}_{10}C_{m-1}$ and x are the combination and isotope labeling ratio, respectively. In 2 spin systems, the probability (P_2) is 12.1%, and there are 10 different spin topologies. Similarly, the number of different spin topologies and the probabilities corresponding with m spin systems are calculated as follows: 45 in 3 spins (P_3 = 23.3%), 120 in 4 spins (P_4 = 26.7%), 210 in 5 spins (P_5 = 20.0%), 252 in 6 spins (P_6 = 10.3%), 210 in 7 spins (P_7 = 3.7%), 120 in 8 spins, 45 in 9 spins, 10 in 10 spins, and 1 in 11 spins ($\Sigma_{m=8}^{11}P_m$ = ~1.0%). In these m spin systems, individual sub-buildup curves for different topologies are simulated on the basis of atomic coordinates determined by XRD.[20] Different spin topology, internuclear distances, and coupled spin numbers lead to different buildup curves. Increasing the spin number gives faster buildup (Figure S3, Supporting Information). Individual curves are summed up by weighting probability (w_{m_i}) to find the spin topology in m spins. Subsequently, individual summed DQ sub-buildup curves for m spin systems are further weighted by P_m (Figure 2(c)). $\Sigma_{m=8}^{11}P_m$ is ~1.0%, and the DQ curve for 6 spins is almost the same as 7 spins (Figure S3(g), Supporting Information). Thus, it is approximated that the DQ curves for higher spin interactions of more than 8 spins are assumed to be the same as the 7 spins (yellow line in Figure 2(c)). Additionally, the resulting DQ curves were modulated by a damped T_2 value. Thus, all possible spin interactions (the shortest distance of 4.2 Å) and exponential type of T_2 = 24 ms lead to one simulated DQ curve (blue line) (Figure 2(d)). The fitted curve has a slightly slower buildup than the experimental one. Thereby, closer chain packing was further investigated by changing atomic coordinates along the a and b axes equally. The best fitting curve to the experimental data has the shortest distance and relaxation value of 4.0 ± 0.2 Å and T_2 = 18.5 ± 1 ms, respectively (red line in Figure 2(d)). Similar results were obtained in analyses of the packing structures of *isotactic* poly(propylene) (iPP).[23−26] Natta et al. for the first time reported the shortest interstem CH_3-CH_3 distance of $\langle r \rangle$ = 4.2 Å for the α form of iPP in 1960.[23] Later, Mencik revised the distance down to 4.0 Å for the α form prepared at moderate annealing temperature.[24] Hikosaka et al. reported $\langle r \rangle$ = 3.8 Å for α from annealing at very high temperature close to melting temperature.[25] Also, Cheng et al. reported that a higher iPP

dx.doi.org/10.1021/mz300630j | *ACS Macro Lett.* 2013, 2, 501−505

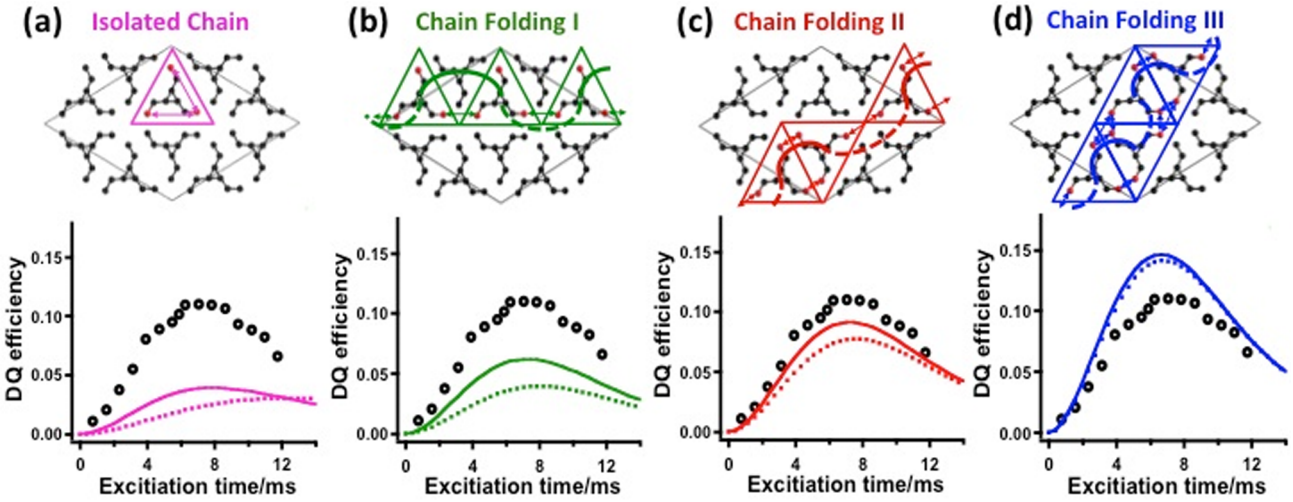

Figure 3. Experimental $^{13}C-^{13}C$ DQ buildup curves of ^{13}C-labeled and nonlabeled blended form I iPB1 at 1:9 mixing ratio (○) and calculated ones based on four possible chain-folding (CF) models such as (a) isolated Chain (CF0), (b) CFI, (c) CFII, and (d) CFIII. The dotted and solid curves corresponding to pure intrachain and intra- and interchain effects, respectively. The CFI, CFII, and CFIII have the chain-folding number of 4.

provides closer packing in the α form.[26] These results would support a closer packing structure of iPB1 in current work than that by Natta et al.[20] All the atomic coordinates and T_2 = 18.5 ms are employed for the best fitting curve and further studying the chain trajectory in iPB1. When the isotopic labeling method is applied to the study of crystalline polymers, segregation effects should be taken into consideration.[27] Segregation effects are investigated through ξ. In 30% ^{13}C-labeled homopolymer, ξ_{max} = 0.23 at 10:0 (the ratio of ^{13}C-labeled:nonlabeled chains) decreases to 0.16, 0.14, and 0.11 at 5:5, 3:7, and 1:9, respectively (see detailed DQ curves in Figure S4, Supporting Information). It was observed that under assumption of single-mixed composition crystals, ^{13}C-labeled and nonlabeled chains cocrystallize at the stem levels even under very slow crystallization at 95 °C (crystallization time of 72 h). Lowering the composition of the labeled polymer changes the majority of DQ signal intensity into intrachain effects from a mixture of inter- and intrachain ones. The chain trajectory of isolated polymer chains can be investigated by DQ NMR under assumptions of statistical interchain effect. Figures 3(a)−(d) show experimental $^{13}C-^{13}C$ DQ curves of ^{13}C-labeled iPB1 diluted with nonlabeled chains (1:9) (open circles) and calculated ones based on four chain-folding models at n = 4. The solid and dotted curves represent calculated DQ buildup with and without statistical interchain effects. Figure 3(a) illustrates the calculated ^{13}C DQ curve of an isolated ^{13}C-labeled chain, named as CF0, which is dominant in the switchboard or random re-entry model. In the isolated chain, long-range distances of $\langle r\rangle$ = 6.3, 6.5, and 7.8 Å contribute to the DQ curve. ξ_{max} are calculated to be 0.015 at t_{ex} = 12.9 ms, 0.028 at 12.5 ms, and 0.030 at 12.5 ms for 3, 5, and 7 spin sites, respectively (see Figure S5, Supporting Information). The result corresponding to 7 spin site systems is shown as a dotted curve in Figure 3(a). In addition to intrachain interactions, statistical interchain effects on the DQ curves are investigated. As discussed in chain-packing analysis, 8 interstem and 1−7 intrastem spin sites are considered. The calculated ξ_{max} of CF0 is 0.033, 0.034, 0.038, and 0.039 at the same t_{ex} = 7.8 ms for intra- and interchain, according to spin numbers of 1, 3, 5, and 7 (pink solid curve in Figure 3(a)), respectively (see Figure S5, Supporting Information). Most of the buildup curves we will deal with have maxima in the range of 6−7 ms. An important perspective is that, in the absence of T_2 effects, the t_{ex} at the maximum in any buildup curve associated with a given dipolar pair is inversely proportional to dipolar interaction. Thus, for most cases considered herein, when the maximum is determined by multiple couplings, the weaker couplings are automatically biased against. The height of the maximum, either experimental or calculated, is weighted more heavily toward the stronger dipolar couplings, which, in this case, originate mainly from interstem dipolar pairs. Therefore, in chain-folding and chain-packing calculations, the closest 2 intrastem ($\langle r\rangle$ = 6.3 Å) and 8 interstem spin interactions ($\langle r\rangle$ = 4.0 and 5.7 Å) are at the most taken into account. Ignoring long-range intrastem interactions may slightly underestimate ξ in subsequent calculations. This effect on DQ efficiency is estimated to be less than 0.005 on the basis of the CF0 model (see Figure S5, Supporting Information). Note that the following calculations include this minor contribution from long-range intraspin effects in the calculated ξ.

The CFI model in Figure 3(b) describes the chain structure folded across the crystallographic a and b axes. Two sites of individual 3_1 helical stems are possible with $^{13}C-^{13}C$ interstem interactions with $\langle r\rangle$ = 4.0 Å, while another is too far ($\langle r\rangle$ = 9.5 Å) to contribute to the DQ signal. The calculated ξ_{max} in the CFI model is 0.062 at t_{ex} = 7.1 ms (green solid curve). In the following CFII and CFIII models, there are several possibilities for CF directions having the same required spin topology. In these cases, DQ NMR no longer specifies the crystallographically preferred chain-folding direction. Two of them are shown in Figures 3(c) and (d). Figure 3(c) shows a CFII model, where the chain-folding direction is along the crystallographic a axis where two sites adopt $\langle r\rangle$ = 4.0 Å and another has 5.7 Å. The simulation of CFII including interchain effects produces a faster DQ buildup curve with ξ_{max} = 0.091 at t_{ex} = 7.4 ms (red solid curve). In a CFIII model, the chain alternately switches folding directions, and all ^{13}C-labeled spins closely interact with those between the adjacent stems. The shortest $\langle r\rangle$ = 4.0 Å and the largest number of coupled spins provide the highest ξ_{max} of 0.146 at t_{ex} = 6.7 ms (blue solid curve). This complex model shows a simulated curve including the interchain effect, which is quite similar to that without the

dx.doi.org/10.1021/mz300630j | ACS Macro Lett. 2013, 2, 501−505

interchain one. Experimental and calculated DQ curves support only the CFIII model to be plausible chain-folding topologies. One may consider different folding models. An additional three models are treated in Figures S6 and S7 (Supporting Information).

Moreover, the n and F effects on ξ are further investigated using the CFIII model. Figure 4(a) shows n effects on ξ under

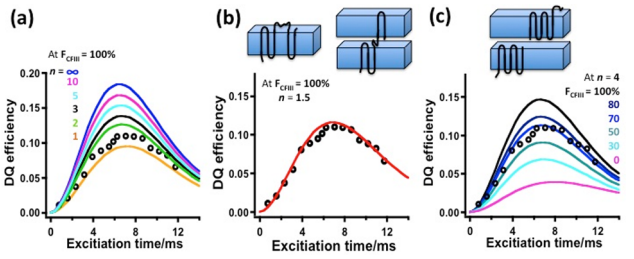

Figure 4. Effects of (a) chain-folding number, n, and (b) n = 1.5 under assumption of F_{CFIII} = 100% on the DQ buildup curve. (c) Effects of adjacent re-entry fraction (F_{CFIII}) at n = 4 on the DQ buildup curve. All results use the CFIII model with possible overall chain structures.

assumption of all chains adopting adjacent re-entry structures (F_{CFIII} = 100%). It is clearly demonstrated that decreasing of n leads to lower ξ_{max}. In real systems, both M_w and $\langle l \rangle$ of the sample crystallized at T_c = 95 °C limit possible n_{max} to be 4. Two parameters of $n \leq 4$ and F_{CFIII} resultantly determine the DQ buildup curve.

Here, two limiting structures providing maximum and minimum F_{CFIII} values are treated. Figure 4(b) shows that the calculated DQ red curve on the basis of combinations (n = 1.5) of n = 1 and n = 2 under F_{CFIII} = 100% is well consistent with the experimental data, where one chain has two adjacent re-entry structures with n = 2 (three stems) and n = 1 (two stems) in the crystalline region. Two different types of overall chain structures are possible to explain the local chain-folding structures, where one chain penetrates either two successive lamellae or one as illustrated in Figure 4(b). Early neutron scattering work on iPP and PE showed one and two stem lengths corresponding to these two models in relatively low M_w samples.[28] Actually, the stem length of the current sample is not known. Thus, we cannot specify either one or two stem lengths. At n = 4, 5 stems are included in adjacent re-entry structures in the same lamellae. F_{CFIII} = 70% (blue) produces the experimental result under the assumption that the remaining 30% of stems adopt CF0 (Figure 4(c)). Actually, intermediate states between two limits would be possible. Thus, it is concluded that F_{CFIII} ranges from 70% at n = 4 to 100% at mixed structures of n = 1 and 2. The proven highly adjacent re-entry fraction also supports roles of intramolecular interaction on nucleation proposed by recent computer simulations.[9,10] Finally, we would like to give comments on chain-folding in form I single crystals of iPB1, which show hexagonal shapes at ca. 10 μm.[29] A loop model of the chain trajectory may explain the hexagonal morphology (see Figure S8, Supporting Information). In this model, if the fourth, fifth, and sixth stems in a CFIII model (Figure 3(d)) occupy open sites toward a filled hexagon, the first loop is closed by 6 stems. Similarly, the s^{th} loop is filled with $(2s - 1) \times 6$ stems. Considering the single crystal sizes and finite folding number (e.g., n = 4), it is understood that most chain trajectories (spin topology) in the outer loops are the same as that in CFIII (Figure 3(d)).

Our experimental results are the first evidence to determine (i) adjacent re-entry fractions and (ii) re-entrance sites under consideration of finite chain-folding numbers. The current NMR approach combined with selective isotopic labeling will clarify chemical and physical effects such as molecular weight, supercooling, and entanglements on chain-level structures in the polymer crystals in the future.

■ ASSOCIATED CONTENT

Supporting Information

Synthesis procedure, preparation of crystal, NMR experimental condition, atomic coordinates, internuclei distance obtained by XRD and NMR, and simulation results. This material is available free of charge via the Internet at http://pubs.acs.org.

■ AUTHOR INFORMATION

Corresponding Author

*E-mail: miyoshi@uakron.edu.

Notes

The authors declare no competing financial interest.

■ ACKNOWLEDGMENTS

This work was financially supported by the National Science Foundation. (Grant no. DMR-1105829). We are greatly indebted to Dr. Jeffrey Quinn and Dr. Michael Davis at Bridgestone USA for GPC measurement and careful reading of our manuscript.

■ REFERENCES

(1) Keller, A. *Philos. Mag.* **1957**, *2*, 1171−1175.
(2) Fisher, E. W. *Pure. Appl. Chem.* **1978**, *50*, 1319−1341.
(3) Sadler, D. M.; Keller, A. *Science* **1979**, *203*, 263−265.
(4) Reddy, K. R.; Tashiro, K.; Sakurai, T.; Yamaguchi, N. *Macromolecules* **2008**, *41*, 9807−9813.
(5) Zeng, X.; Ungar, G.; Spells, S. J.; King, S. M. *Macromolecules* **2005**, *38*, 7201−7204.
(6) Wittmann, J. C.; Lotz, B. *J. Polym. Sci., Polym. Phys. Ed.* **1985**, *23*, 205−226.
(7) Kumaki, J.; Kawauchi, T.; Yashima, E. *J. Am. Chem. Soc.* **2005**, *127*, 5788−5789.
(8) Liu, K.; Song, Y.; Feng, W.; Liu, N.; Zhang, W.; Zhang, X. *J. Am. Chem. Soc.* **2011**, *133*, 3226−3229.
(9) Hu, W. B.; Cai, T. *Macromolecules* **2008**, *41*, 2049−2061.
(10) Luo, C.; Sommer, J. U. *Macromolecules* **2011**, *44*, 1523−1529.
(11) Schmidt-Rohr, K.; Spiess, H. W. *Multidimensional Solid-State NMR and Polymers*; Academic Press: London, 1994.
(12) Mackenzie, K. J. D.; Smith, M. E. *Multinuclear Soild-State NMR of Inorganic Materials*; Elsevier Science Ltd: Amsterdam, 2002.
(13) Mehta, M. A.; Eddy, M. T.; McNeill, S. A.; Mills, F. D.; Long, J. R. *J. Am. Chem. Soc.* **2008**, *130*, 2202−2212.
(14) Gullion, T.; Yamauchi, K.; Okonogi, M.; Asakura, T. *Macromolecules* **2007**, *40*, 1363−1365.
(15) Suzuki, Y.; Aoki, A.; Nakazawa, Y.; Knight, D. P.; Asakura, T. *Macromolecules* **2012**, *43*, 9434−9440.
(16) Brown, S. P.; Spiess, H. W. *Chem. Rev.* **2001**, *101*, 4125−4155.
(17) Caporini, M. A.; Bajaj, V. S.; Veshtort, M.; Fitzpatrick, A.; MacPhee, C. E.; Vendruscolo, M.; Dobson, C. M.; Griffin, R. G. *J. Phys. Chem. B* **2010**, *114*, 13555−13561.
(18) Castellani, F.; Van Rossum, B.; Diehl, A.; Schubert, M.; Rehbein, K.; Oshikinat, H. *Nature* **2002**, *420*, 98−102.
(19) Miyoshi, T.; Mamum, A. *Polym. J.* **2012**, *44*, 65−71.
(20) Natta, G.; Corradini, P.; Bassi, I. W. *Nuovo Cimento* **1960**, *15*, 52−67.
(21) Hohwy, M.; Jakobsen, H. J.; Edé n, M.; Levitt, M. H.; Nielsen, N. C. *J. Chem. Phys.* **1998**, *108*, 2686−2694.
(22) Veshtort, M.; Griffin, R. G. *J. Magn. Reson.* **2006**, *178*, 248−282.

(23) Natta, G.; Corradini, P. *Nuovo Cimento* **1960**, *15*, 40−51.
(24) Mencik, Z. *J. Macromol. Sci., Part B: Phys.* **1972**, *B 6*, 101−105.
(25) Hikosaka, M.; Seto, T. *Polym. J.* **1973**, *5*, 111−127.
(26) Janimak, J. J.; Cheng, S. Z. D.; Zhang, A.; Hsieh, E. T. *Polymer* **1992**, *33*, 728−735.
(27) Stehling, F. C.; Ergos, E.; Mandelkern, L. *Macromolecules* **1971**, *4*, 672−677.
(28) Ballard, D. G. H.; Longman, G. W.; Crowley, T. L.; Cuningham, A.; Schelten, J. *Polymer* **1979**, *20*, 399−405.
(29) Zhang, B.; Yang, D.; Yan, S. *J. Polym. Sci., Part B: Polym. Phys.* **2002**, *40*, 2641−2645.